Higher Order Structure Contributes to Specific Differences in Redox Potential and Electron Transfer Efficiency of Root and Leaf Ferredoxins†

Ping Gou,‡,§ Guy T. Hanke,*,‡ Yoko Kimata-Ariga,‡ Daron M. Standley,‡ Atsushi Kubo,|| Isao Taniguchi,|| Haruki Nakamura,‡ and Toshiharu Hase‡

Institute for Protein Research, Osaka University, 3-2 Yamadaoka, Suita, Osaka 565-0871, Japan, and Department of Applied Chemistry and Biochemistry, Kumamoto University, 2-39-1 Kurokami 860-8555, Japan

Received August 28, 2006; Revised Manuscript Received September 29, 2006

ABSTRACT: Plant type ferredoxin (Fd) is a small [2Fe-2S] cluster containing electron-transfer protein with a highly negative redox potential. Higher plants contain different iso-protein types of Fd in roots and leaves, reflecting the difference in redox cascades between these two tissues. We have combined subdomains of leaf and root Fds in recombinant chimeras, to examine structural effects and the relationship between groups of residues on redox potential, electron transfer, and protein−protein interactions. All chimeras had redox potentials that were intermediate to the wild type leaf and root Fds. Surprisingly, the largest differences resulted from exchange of the N-terminus, the region farthest from the redox center. Homology modeling and energy minimization calculations suggest that the N-terminal chimeras may indirectly influence redox potentials by structurally perturbing the active site. Measurements of electron transport and protein interaction indicate that synergistic interaction between the C- and N-terminal of root Fd bestows a specific high affinity for accepting electrons in the root type electron cascade, and that there is discrimination against photosynthetic electron donation to root Fd based on the C-terminus of the molecule. Taken together, the experimental and computational studies support a model in which higher order structure contributes to iso-protein specific interaction and electron-transfer properties.

Plant-type ferredoxin (Fd[1]) is a soluble 11 kDa electron-transfer protein, whose [2Fe-2S] cluster confers a highly negative redox potential (*1*). Fd is best known for accepting electrons from photosystem I (PSI) and donating them to Fd-$NADP^+$ reductase (FNR, EC 1.18.1.2) for photoreduction of $NADP^+$ (*2*), but it also supplies reducing power to many other enzymes of biosynthesis and bioassimilation (*3*). In order that these reactions can continue under non-photosynthetic conditions, such as in the dark or in roots, Fd is reduced by NADPH oxidation, in a reversal of the FNR reaction (*4*).

Higher plants contain distinct leaf and root iso-forms of Fd (*5*, *6*) with conserved differences (Figure 1A), reflecting the different electron donors to Fd in photosynthetic and non-photosynthetic tissues. Functional differences have been demonstrated between leaf and root Fds, with respect to redox potential and activity in assays of $NADP^+$ photoreduction and NADPH oxidation (*7*−*9*). These differences are highly conserved across species boundaries (*7*, *8*): Leaf Fds have redox potentials around 50 mV more negative than root Fds; during $NADP^+$ photoreduction, leaf FNR has a K_m around 10-fold lower for leaf Fds than for root Fds, and during NADPH oxidation root FNR has K_m values around five times lower for root Fds than for leaf Fds. As the redox potential of leaf Fd is around −420 mV, a 50 mV difference does not initially appear dramatic, but the flux through photosynthesis is so vast that small changes in efficiency are likely to have a profound physiological impact. In addition, the concentration of Fd in the chloroplast is of the same order as the concentration of Fd dependent enzymes (*10*, *11*), which will therefore effectively be in competition, giving great physiological significance to even small differences in affinity and activity.

Fd molecules have been very well characterized, with site directed mutagenesis (*9*, *12*−*15*) and computer modeling (*16*) studies helping to determine specific residues that contribute to their redox properties. In addition, X-ray crystal structures of complexes between leaf Fd and leaf FNR and between root Fd and root FNR from maize have been solved (*8*, *17*, *18*) and, in conjunction with site directed mutagenesis studies (*9*, *14*, *15*, *19*), reveal which Fd residues are important for binding FNR. However, all Fd residues found to contribute to intermolecular ionic bridging are conserved between leaf and root type Fds, so the basis for iso-protein specific K_m differences remains unclear.

The difference in redox potential between [2Fe-2S] cluster proteins is thought to be due to electrostatic interactions between the polypeptide environment and the active site cluster (*20*). However, the primary sequence and three-

† This work was partly supported by Grant in Aid 15GSO320 for Creative Science, and by Grant in Aid 18770035 for Young Scientists B from the Ministry of Education, Culture, Sports, Science and Technology of Japan.

* Corresponding author. Tel: +81-6-6879-8611. Fax: +81-6-6879-8613. E-mail: enzyme@protein.osaka-u.ac.jp.

‡ Osaka University.

§ Current address: College of Life Science and Technology, Xingjiang University, Urumchi 830046, P. R. China.

|| Kumamoto University.

[1] Abbreviations: Fd, ferredoxin; FNR, ferredoxin-$NADP^+$ reductase (EC 1.18.1.2); PS, photosystem; 3-D, three-dimensional; cyt *c*, cytochrome *c*; AtFd2, *Arabidopsis* leaf type ferredoxin; AtFd3, *Arabidopsis* root type ferredoxin; MD, molecular dynamic; NER, number of equivalent residues.

10.1021/bi061779d CCC: $33.50
Published on Web 11/09/2006

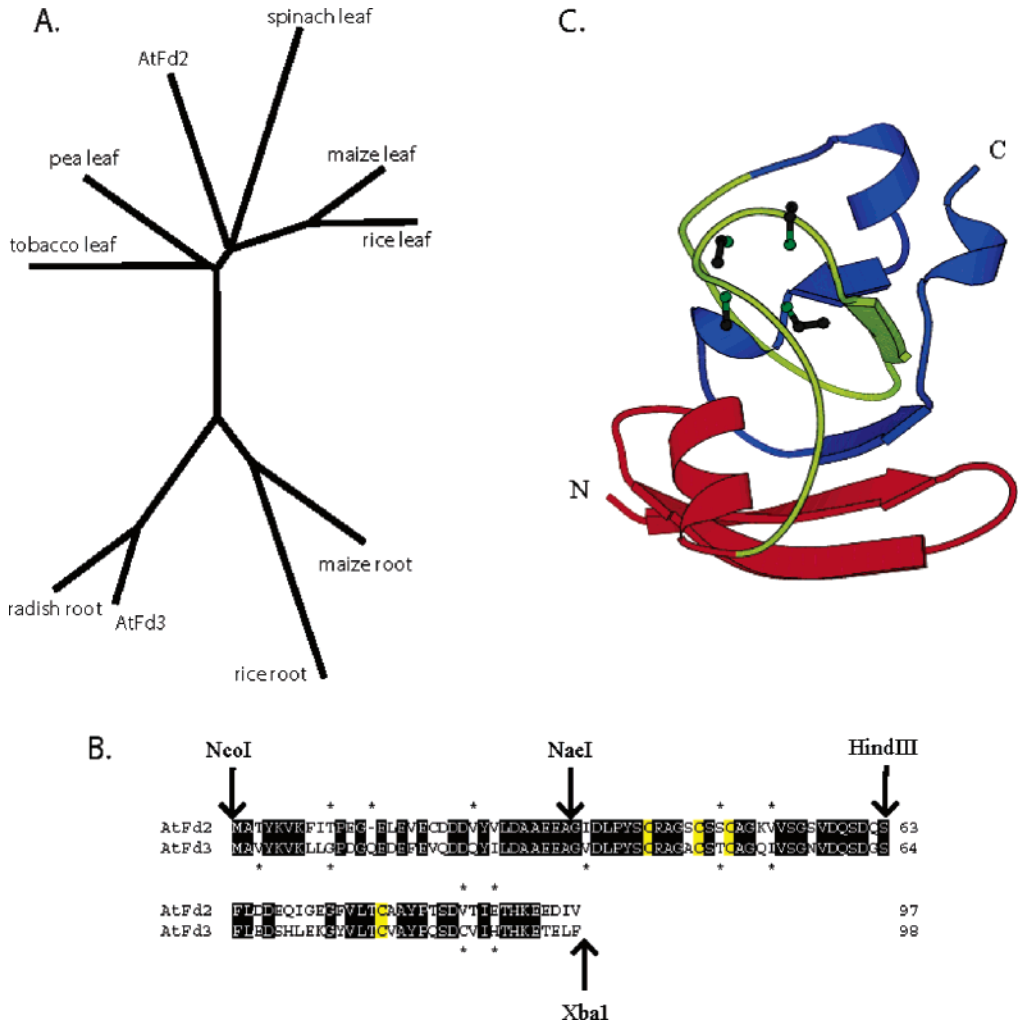

FIGURE 1: A comparison of leaf and root type Fds. (A) A phylogenetic tree of leaf and root Fd amino acid sequences from several higher plants, including *Arabidopsis* leaf (AtFd2) and *Arabidopsis* root Fd (AtFd3), was drawn by aligning the sequences in ClustalW 1.8 (http://www.ebi.ac.uk/clustalw/). (B) AtFd2 and AtFd3 amino acid sequences were aligned in ClustalW 1.8. Identical residues are shown as white on black, and [2Fe-2S] cluster ligating cysteines are black on yellow. Asterisks above the line mark residues conserved among typical leaf Fds, but absent from root Fds, and asterisks below the line show residues conserved among typical root Fds, but absent from leaf Fds. The positions of restriction sites on the equivalent nucleotide sequence used to digest original Fd plasmids and create chimeras are indicated. (C) Ribbon diagram of maize (*Zea mays*) root Fd III structure (PDB under submission). The [2Fe-2S] cluster is shown as red balls. The regions with blue, yellow, and green colors correspond to the N-, middle, and C-terminal subdomains of the Fd chimeras respectively.

dimensional (3-D) structures of leaf and root Fd are very similar (*8*, *17*, *18*, *20*). This is particularly true for the active site regions, so the basis of the functional differences between leaf and root Fd remains obscure. Indeed, from the wealth of information on the amino acids that define fundamental Fd-like parameters, only one, T48S (*Arabidopsis* root Fd nomenclature), which determines a small change in redox potential in the cyanobacterium *Anabaena* Fd, has distinct conservation in root/leaf type Fds (*14*).

Anabaena has vegetative (VFd) and heterotrophic (HFd) Fds, which are approximately homologous in function to higher plant leaf and root types respectively. VFd has a redox potential 33 mV more negative than HFd, and the effect of exchanging VFd and HFd residues in the cluster binding loop has been investigated (*14*), but in no case could site directed mutagenesis of these amino acids reconcile the difference in potential between VFd and HFd. Moreover, exchange of single amino acids between [4Fe-4S] Fds of *Azobacter vinelandii* and *Peptococcus aerogenes* (*21*), which vary in redox potential by more than 200 mV, failed to identify any determinants for this difference in potential, the only small shift being on a substitution of F25I that resulted in significant structural changes.

These results suggest that structural interaction between larger groups of residues could contribute to the fine-tuning of Fd redox potential and interactions with FNR, ensuring differentiation and therefore optimum function of the leaf and root Fd iso-proteins. We previously examined the functional characteristics of the major leaf type and root type Fd species from *Arabidopsis* (*8*), and here we present analysis of chimeric molecules constructed by combining homologous subdomains of the two wild type proteins. This allowed us to study the relationship between Fd subdomains and properties such as redox potential, electron transfer, and protein affinity. Structural effects are also investigated by simulating the perturbation to the wild type proteins induced by the chimeric sequences through a combination of homology modeling and energy minimization.

EXPERIMENTAL PROCEDURES

Gene Construction, Recombinant Expression, and Purification of Chimeric Mutants of AtFd2 and AtFd3. Plasmids

containing six chimeric AtFd genes were produced from plasmids (pTrc99A, Amersham) containing the AtFd2 and AtFd3 genes prepared previously (*8*), by ligating cleaved AtFd2 fragments into AtFd3 plasmids digested with the same restriction enzymes (*Nco*I/*Hin*dIII, *Nae*I/*Hin*dIII, or *Nae*I/*Xba*I), and vice versa (Figure 1B) to create constructs of all possible combinations of the Fd subdomains. The chimeric AtFd mutant proteins were expressed in *Escherichia coli* JM105 and then purified essentially as described by Akashi et al. (*9*).

Physicochemical Analysis. Native gradient PAGE was performed as described by Kimata and Hase (*22*). Redox potentials were calculated as the midpoint of cyclic voltammetric measurements made at 25 °C versus a standard hydrogen electrode at pH 7.5 essentially as described by Taniguchi et al. (*12*).

Affinity Chromatography. AtFds were immobilized on CNBr-activated Sepharose 4B, and chromatography was performed essentially as described by Onda et al. (*7*) except that 2.2 nmol of each maize FNR iso-protein was loaded on the column, and a linear gradient of NaCl from 0 to 300 mM in 50 mM Tris-HCl, pH 7.5 was applied to elute proteins at a flow rate of 0.5 mL/min.

Enzymatic Analysis. Measurements of NADPH-dependent cytochrome *c* (cyt *c*) reduction by FNR iso-proteins were performed as described by Onda et al. (*7*). Photosynthetic $NADP^+$ reduction using spinach thylakoid membranes was measured as described by Hanke et al. (*8*).

Structural Modeling. Homology models of leaf and root AtFd were built using the corresponding maize structures (PDB IDs 1gaw and PDB file under submission, respectively) as templates following a BLAST sequence alignment, and did not include the [2Fe-2S] cluster. Initially, the backbone and side chains of all common residues were fixed to the template values. Missing residues were then introduced one at a time by searching the Protein Data Bank for side chain conformations that minimized atomic clashes with the rest of the structure. The resulting leaf and root AtFd models were then structurally superimposed using the program GASH (*23*), allowing the initial chimeric models to be built by directly swapping the appropriate fragments. The initial models were then relaxed via a short (1 ns) annealed molecular dynamics (MD) simulation in which the temperature was lowered from 300 to 10 K. The higher temperature allows initial structures to escape from energetically unfavorable conformations introduced by homology building and subdomain swapping. The lower temperature traps low energy states at the end of the simulation. The minimized chimeric structures were then structurally superimposed on the minimized wild type structures, and the degree of structural similarity and dissimilarity upon relaxation was computed. Each MD run was repeated 15 times for every initial structure using different random initial velocities in order to obtain the average similarity and dissimilarity overall and per residue. All MD calculations were performed using the *cosgene* program in the *PrestoX* simulation package (*24*). Structural similarity was defined using the number of equivalent residues (NER) (*25*), which is bounded between zero and the number of residues in the shortest chain. The dissimilarity was given by the Euclidian distance between C_α atoms.

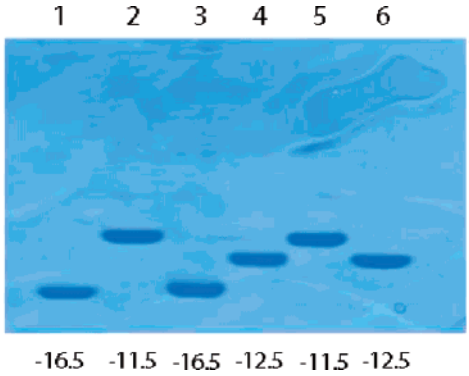

FIGURE 2: Separation of purified wild type and chimeric AtFd proteins by native gradient PAGE. Five micrograms of protein was loaded in each lane. Lanes were 1, AtFd2; 2, AtFd223; 3, AtFd322; 4, AtFd233; 5, AtFd323; 6, AtFd3. The numbers below each lane represent the net charge of the corresponding Fd calculated on the assumption that each acidic residue (Asp and Glu) confers one negative charge, each basic residue (Lys and Arg) confers one positive charge, and His residue is 0.5-positively charged.

Redox Potential Prediction. The redox potentials of the chimeric proteins were predicted by a weighted sum of the original leaf and root redox potentials (V^0_{leaf} and V^0_{root}, respectively), with the weights given by the degree of structural similarity to the original structures. Given leaf and root similarity values, NER_{leaf} and NER_{root}, the redox potential for a given chimeric protein was predicted to be

$$V^0_{pred} = \frac{V^0_{leaf}\,NER_{leaf} + V^0_{root}\,NER_{root}}{NER_{leaf} + NER_{root}} \qquad (1)$$

RESULTS

Design and Expression of Chimeric Molecules Composed of Leaf and Root Type Fds. We previously constructed plasmids for recombinant expression in *E. coli* of *Arabidopsis thaliana* leaf type Fd (AtFd2) and root type Fd (AtFd3) (*8*). Their amino acid sequences are highly homologous, allowing simple insertion of restriction sites at exactly equivalent positions in the coding DNA sequence. Fd is a small, compact protein, and there are no obvious candidates for domain exchange, although the central portion of the molecule contributes 3 of the 4 cysteine residues that coordinate the [2Fe-2S] cluster in a cluster binding loop. We therefore defined three subdomains within Fd of approximately 30 amino acid each (Figure 1B, 1C). The resulting N-terminal, central, and C-terminal subdomains of AtFd2 and AtFd3 are 64%, 77%, and 53% identical respectively, and all contain residues exclusive to, and conserved among, either root or leaf type Fds (Figure 1B). Plasmid DNA encoding all possible chimeric combinations of these subdomains were constructed, and introduced into *E. coli*.

All chimeras could be assembled into the holo form following expression in *E. coli*, except those containing the combination of the AtFd3 central subdomain and AtFd2 C-terminal subdomain (AtFd232 and AtFd332). The other four chimeras were purified to homogeneity, and their absorption spectra in the visible region were essentially the same as those of the parental Fds, indicative of correct assembly of the [2Fe-2S] cluster. A comparison of their migration through native PAGE is shown in Figure 2, being approximately proportional to net charge at pH 7.5.

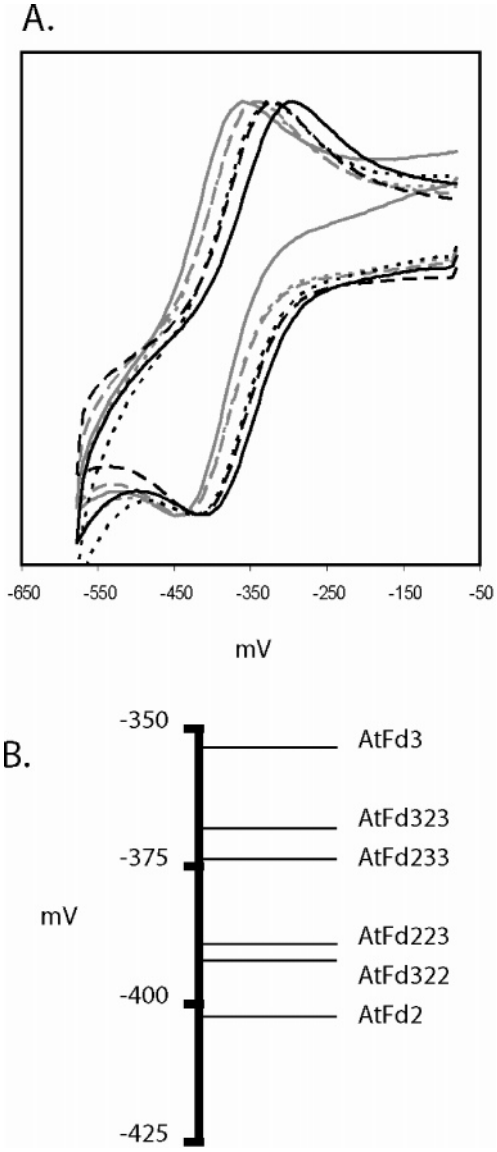

FIGURE 3: Comparison of redox potentials of wild type and chimeric AtFd proteins. (A) Cyclic voltammograms taken in 100 μM solutions of AtFd2 (solid gray line), AtFd223 (hashed gray line), AtFd233 (dotted gray line), AtFd322 (dotted black line), AtFd323 (hashed black line) and AtFd3 (solid black line): current (nA) versus a standard hydrogen electrode potential. Results are typical of at least three independent measurements. (B) Comparison of the average midpoint potentials of chimeric and wild type AtFd proteins. Potentials were −354, −369, −374, −390, −393, and −403 mV for AtFd3, 323, 233, 223, 322, and Fd2, respectively. SD was less than 2 mV in all cases.

Additive Effect of the Fd Subdomains on Redox Potential Shift of the [2Fe-2S] Cluster. Redox potentials of Fd were taken as the midpoint potential over cyclic voltammetry (Figure 3A), and potentials of AtFd2 and AtFd3 were consistent with previous measurements. The potentials of all chimeric molecules were intermediate, with the difference from the potentials of parental molecules roughly proportional to the relative composition of AtFd2 and AtFd3 subdomains (Figure 3B). These results suggest that each subdomain exerts an influence on the active site environment. Most remarkably, although the N-terminal subdomain has no direct contact with the [2Fe-2S] cluster, its exchange causes a significant shift in redox potential (−20 mV relative to AtFd3 and +10 mV relative to AtFd2).

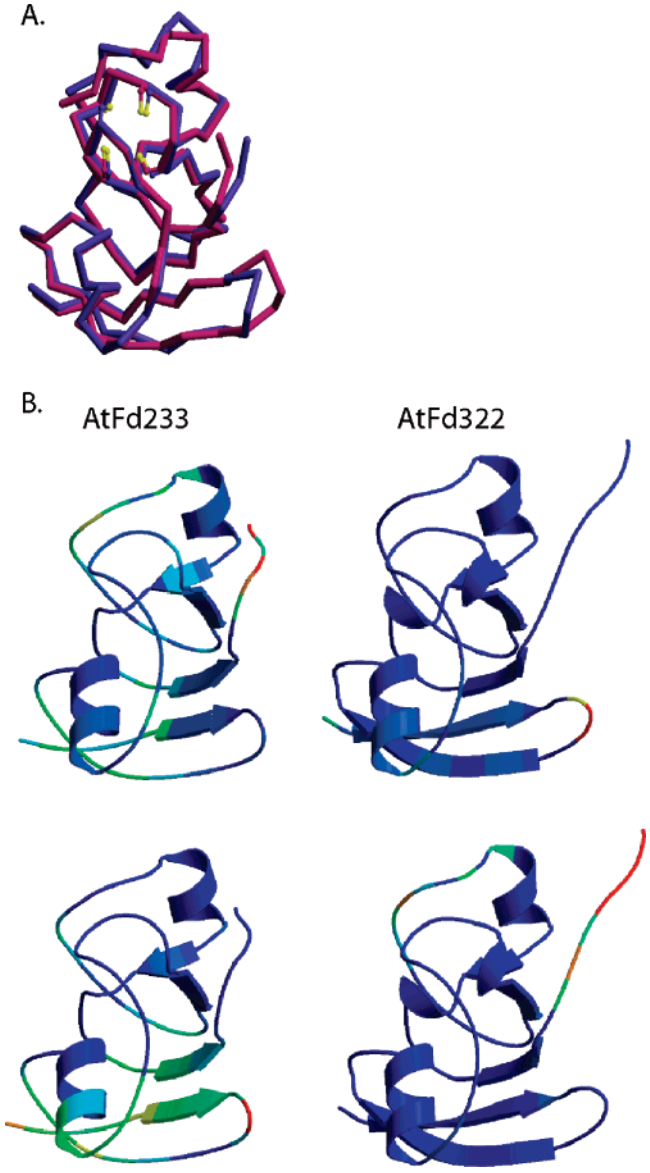

FIGURE 4: Structural changes from initial models upon MD relaxation. (A) Superimposition of the modeled AtFd2 (blue) and AtFd3 (red) structures. (B) Structural variation (blue → red = increasing variation) from AtFd2 (upper panel) and AtFd3 (lower panel) on exchange of the N-terminal. For each homology model the structures before and after the MD simulation were superimposed and the distance between corresponding C_α atoms was computed. The figure shows the average distance over 15 MD runs.

Structural Modeling Suggests That Overall Backbone Folding Contributes to Redox Potential Difference. To investigate the origins of chimeric substitution effects on redox potential, we modeled the perturbations to the wild type structure induced by subdomain exchange. Homology modeling of AtFd2 and AtFd3 was carried out using coordinates from maize leaf and root Fd respectively, and the resulting AtFd2 and AtFd3 structures are shown in Figure 4A. Subdomains of these structures were combined directly to form chimeras, and structural similarity to both the relaxed AtFd2 and AtFd3 models was computed following relaxation of each chimera.

Structural perturbation has been linked with changes in the redox potential of [4Fe-4S] Fds (*21*). We therefore examined whether exchange of one Fd subdomain caused structural changes in other areas of the protein molecule,

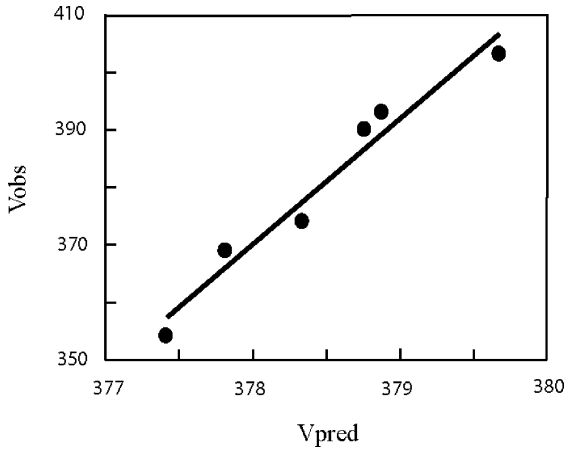

FIGURE 5: Correlation between observed and predicted redox potentials. The observed redox potentials of wild type and chimeric AtFd proteins are plotted against the values predicted using eq 1.

with particular reference to exchange of the N-terminal region. Figure 4B shows the structural deviation from parental structures on models of chimeras with exchanged N-termini (deviation from on a per-residue basis is shown in the Supporting Information). These models predict that exchange of one subdomain will induce structural changes in other Fd subdomains. For example, the greatest shift in redox potential was caused by introduction of the AtFd2 N-terminal subdomain into the AtFd3 molecule. The MD simulation predicts that such an exchange would cause profound differences from AtFd3 structure, far from the N-terminal region. Such perturbation includes residues in the microenvironment of the cluster (e.g., 59−60 and 90). Reciprocal introduction, of the AtFd3 N-terminal into the AtFd2 molecule, also shows structural disruption, resulting in a +10 mV shift in redox potential (Figure 3B). These modeling studies suggest that residue changes far from the redox center have the potential to affect the microenvironment of the [2Fe-2S] cluster through distortion of the spatial distribution of atoms near the active site.

The models were constructed without the [2Fe-2S] cluster, which probably stabilizes the active site to some degree, through covalent bonding with sulfur atoms of ligating cysteines. To investigate whether modeling of Fds without the cofactor resulted in enhanced structural perturbation, we repeated simulations with inter-residue distances between the sulfur-binding cysteine side chain atoms (for atoms with distances <5 Å) restrained to their initial values (in the cluster containing maize Fd crystal structures). These constrained models gave basically the same results as unconstrained models.

Given the apparent additivity of the different subdomains toward the net redox potential, we sought to quantify the contribution from each subdomain. We treated the chimeric sequence as a perturbation to the wild type structure, and examined how each chimera reacted structurally upon relaxation. Because the wild type AtFd structures were also homology models, we computed the structural similarity and difference of each relaxed chimera relative to each relaxed parent. We found that the relative structural similarity to each parent was directly proportional to the corresponding similarity in redox potential. This relationship, expressed in eq 1, and plotted in Figure 5, has a correlation coefficient of 0.98 with respect to the observed redox potentials. For models in

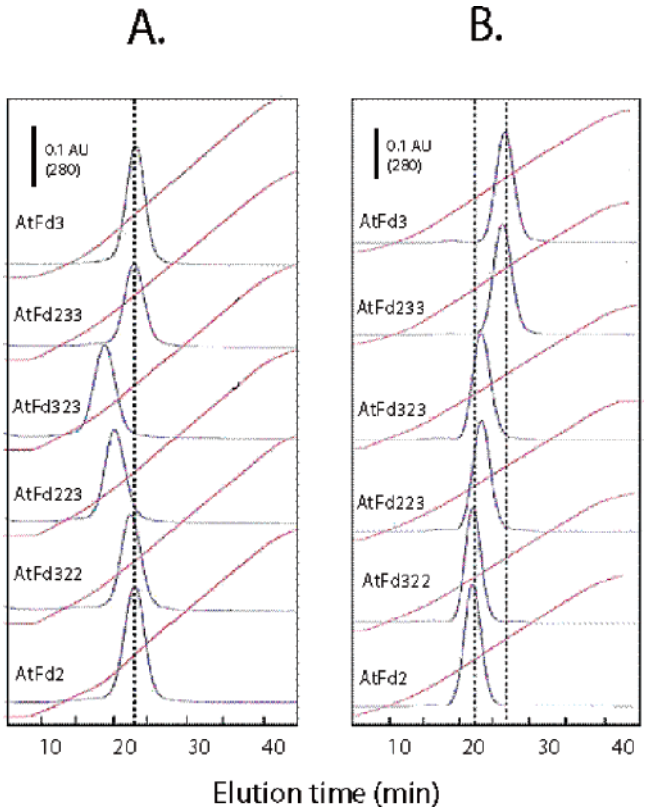

FIGURE 6: Affinity chromatography of leaf type FNR (A) and root type FNR (B) on wild type and chimeric Fd-immobilized Sepharose columns. Leaf FNR or root FNR (2.2 nmol each) were applied to each column and eluted over a linear NaCl gradient of 0−0.3 M in 50 mM Tris-HCl, pH 7.5. Changes in A_{280} and conductivity, recorded during each chromatography, are shown as blue and red curves, respectively. Hashed lines represent the elution point of parental (AtFd2 and AtFd3) molecules for comparison.

which cluster ligating cysteines were constrained, the correlation coefficient dropped slightly to 0.97.

Certain Chimeric Combinations Result in Weaker Interaction with Leaf Type FNR. To examine the contribution of Fd subdomains to differential activity with electron-transfer partners, we measured static interactions of Fds with leaf type and root type FNR enzymes (Figure 6), and their ability to receive electrons from leaf type (nondiscriminatory) and root type (discriminatory) FNR, and transfer electrons between PSI (discriminatory) and leaf type FNR (Table 1).

Ionic interactions with nondiscriminatory (leaf) FNR were only disrupted for chimeric Fds comprising the C-terminus of AtFd3 and the central subdomain of AtFd2 (AtFd323 and AtFd223) (Figure 6A). This correlates directly with the reduced affinity of these Fds in receiving electrons from leaf FNR. Such electron flow is in the opposite direction to that in photosynthesis (where Fd donates electrons to FNR), and so may not relate to in vivo activity, but the K_m of these Fds for the physiologically relevant transfer of electrons from PSI to leaf FNR also increased, most likely due to the same disruptive effects.

The C-Terminal Subdomain Is Crucial for Interaction with PSI. It has previously been reported that transfer of electrons from PSI to leaf FNR is mediated more efficiently by leaf type than root type Fds (*6*, *8*), and this proved to be the case in our measurements. The only chimera to show affinity equivalent to that of leaf Fd contained the C-terminal subdomain of leaf Fd (Table 1). This region has previously

Table 1: Kinetic Parameters of FNR Iso-Enzymes for Fds during NADPH Oxidation, and of Photosystem I and Leaf Type FNR for Fds during $NADP^+$ Photoreduction[a]

	leaf FNR		root FNR		photosystem I	
Fd species	K_m μM Fd	V_{max} μmol of cyt *c* (μmol of enzyme)$^{-1}$ s^{-1}	K_m μM Fd	V_{max} μmol of cyt c (μmol of enzyme)$^{-1}$ s^{-1}	K_m μM Fd	V_{max} μmol of NADPH (μg of chlorophyll)$^{-1}$ s^{-1}
AtFd3	4.8 ± 0.7	76 ± 1	6.0 ± 0.2	212 ± 4	2.4 ± 1.1	0.022 ± 0.008
AtFd233	4.3 ± 0.5	77 ± 1	10.9 ± 0.9	226 ± 10	1.5 ± 0.8	0.032 ± 0.012
AtFd323	8.6 ± 0.1	79 ± 1	4.8 ± 0.3	199 ± 2	2.1 ± 0.8	0.024 ± 0.008
AtFd223	16.3 ± 1.8	72 ± 4	20.9 ± 2.2	233 ± 15	2.1 ± 0.8	0.027 ± 0.012
AtFd322	4.3 ± 0.5	88 ± 3	24.5 ± 1.9	234 ± 5	0.36 ± 0.1	0.023 ± 0.007
AtFd2	5.8 ± 0.2	97 ± 2	26.7 ± 2.7	232 ± 13	0.36 ± 0.1	0.025 ± 0.008

[a] Enzyme assays were performed to measure NADPH-dependent cytochrome *c* (cyt *c*) reduction catalyzed by different FNR iso-forms, and photosynthetic $NADP^+$ reduction by photosystem I and FNR in thylakoid membranes, as mediated by wild type and chimeric AtFds. ±SE.

been implicated in the association of Fd with the PsaD subunit of PSI (*26*), and our results confirm this role, while indicating that PSI discriminates between electron donation to leaf and root type Fds based on the composition of this C-terminal subdomain.

Electron Transfer between Root-Type Fd and Root-Type FNR Is Not Necessarily Correlated with Ionic Interaction. Root type FNR discriminates between Fd types, preferentially donating electrons to root Fd (*7*, *8*) and showing a stronger static, ionic bridge based interaction with root Fd (*7*). The only chimera which retains ionic interaction with root FNR equivalent to that of root type Fd is AtFd233 (Figure 6B), whereas the only chimera which retains high affinity for receiving electrons from root type FNR is AtFd323 (Table 1). The column chromatography used in this interaction study mainly measures ionic effects on static interaction, and it has been shown that, although these dominate the initial, nonproductive complex between Fd and FNR (*19*), the kinetically active complex likely involves several other interactions, such as hydrogen bonding and hydrophobic forces. This variation between strength of interaction and activity is therefore probably due to differential capacity of these two chimeras to form initial and kinetically competent complexes with FNR. The contribution of the C- and N-terminal domains to the high affinity of the AtFd323 chimera in receiving electrons from root FNR appears synergistic, with neither domain alone (AtFd223 or AtFd322) causing a significant difference in affinity from leaf type Fd (Table 1).

DISCUSSION

The leaves and roots of higher plants contain different iso-proteins of Fd, with highly conserved differences in redox potential and enzyme affinity that ensure they function optimally in the different electron-transfer cascades of these tissues. Although extensive research has identified universally conserved amino acid residues responsible for fundamental Fd function, the specific factors that fine-tune the redox potentials and interaction capacities of leaf and root type Fds are not well understood.

The difference in redox potential of various [2Fe-2S] proteins has been explained in terms of a dependence on the electrostatic environment of the active site (*21*). It follows that the environment will in turn depend on both the identity and spatial position of atoms near the [2Fe-2S] cluster. Since mutations near the active site would, in general, result in dramatic functional changes, they are not likely to be tolerated. On the other hand, mutations distant from the [2Fe-2S] complex might generate more subtle or indirect changes. Modeling results in Figure 4B suggest that Fd subdomains removed from the redox center have the capacity to influence active site structure.

With respect to redox potential, introduction of the AtFd2 central domain (containing the cluster binding loop) into AtFd3 caused a −15 mV shift. A single residue change (T48S) may be responsible for this, because the same mutation causes a −15 mV shift in *Anabaena* VFd (*14*). This residue is heavily implicated in the electron-transfer process (*16*). To our surprise, in all other cases, exchange of either the C- or N-termini caused shifts to intermediate redox potentials roughly proportionate to the ratio of AtFd2:AtFd3 subdomains in the molecule. The greatest single difference in redox potential is caused by exchange of the region farthest from the redox center (introduction of the AtFd2 N-terminal to AtFd3). This is presumably due to changes far from the active site inducing structural perturbation around the [2Fe-2S] cluster, an explanation that is consistent with our modeling results. The additive contribution of different subdomains to tuning redox potential, and the linear correlation of redox potential with structural similarity to wild types, is probably coincidental, and may be related to the relatively small size and compact structure of ferredoxin. Whether this behavior is a general property of Fd proteins or a special case of these particular chimeras is a subject for future work.

As we modeled the proteins without the [2Fe-2S] cluster, it is possible that structural changes observed in the active site of our models may not accurately reflect those in the experimental proteins. However, when modeling was repeated with the ligating cysteines restrained to the same position as in crystal structures of cluster containing Fds, we achieved basically the same result. Moreover, the parental AtFd molecules, with which the chimeras are compared, were also modeled without the cofactor.

Chimeric Fds also provided insight into interaction with partner enzymes, and demonstrated that although redox potential may play a role, Fd iso-protein specific enzyme interactions are also dependent on residue/structural interactions between proteins. It has previously been shown that the C-terminus of Fd is directly involved in associating with the PsaD subunit of PSI during photosynthesis (*16*), and the only chimera with the AtFd2 C-terminal subdomain was also the only chimera to retain leaf Fd type high affinity in $NADP^+$ photoreduction. This suggests that PsaD may

discriminate between leaf and root Fds based on specific residues or structures at their C-termini.

Root type FNR has a stronger interaction with, and higher affinity for reduction of, root Fd than leaf Fd (*7*, *8*). Despite this, the Fd residues that form ionic bridges with root FNR in the crystal structure of their complex are conserved among leaf and root type Fds (*18*). Our results indicate that these two forms of discrimination are independent of each other, with the combined C-terminal and central subdomains ensuring high ionic interaction with root FNR, presumably in the initial, nonproductive complex (*19*), while a combination of the C-terminal and N-terminal domains, acting synergistically, is necessary to ensure root Fd like high affinity in accepting electrons. In both cases we assume that these differences relate to achieving an optimal surface topography for binding, and release following electron transfer.

It is not yet clear why two of the chimeras, AtFd232 and AtFd332, could not be assembled into the holo form. In all Fd structures, the C-terminal domain folds back through the central domain, and the high identity between AtFd2 and AFd3 may not be enough to prevent disruption of this intimate relationship. Indeed, the reciprocal combinations (AtFd323 and AtFd223) are unique in their impaired ionic interaction with both FNRs (Figure 6) suggesting relatively large perturbations in structure. The nonbonded electrostatic energy terms are uniformly higher for the nonfolding chimeras, by 400−1400 kcal/mol compared with the other chimeras. Moreover, the nonfolding chimeras have a more negative net charge than any of the other proteins (−17.5, compared to the figures given in Figure 2), suggesting that charge−charge interactions may play a destabilizing role.

Our principal finding is that factors in the N-terminal, distant from the [2Fe-2S] cluster, play a large role in tuning the redox potential of the cofactor, and modeling suggests that this may be through structural perturbation. However, the structural mechanism remains unclear and work to resolve this is ongoing. One of the limitations of the described method of redox potential prediction is that it relies on structural differences between the isoforms. In the case of point mutations that have a significant effect on redox potential, direct solvation of the Poisson−Boltzmann equation to determine the local electrostatic field at the redox center is expected to be a more sensitive method for predicting changes in redox potential, and a combined approach will be developed in future studies.

In conclusion, previous studies on mutagenesis of individual amino acids, or even groups of residues, close to the redox and enzyme binding sites have proved insufficient to explain highly conserved differences between leaf and root type Fds. We have studied chimeric combinations of leaf and root type Fds, and our results indicate that such differences, which ensure that molecules in leaves and roots are optimal for their respective functions, are at least partly due to fine-tuning of higher order structure, with changes far from the active site capable of modifying the properties of the redox center. These findings indicate an avenue of research into the evolutionary differentiation of homologous proteins to perform different functions, with particular reference to subtle differences in redox potential. The construction of chimeric molecules, recombinantly and by structural modeling, has proved a useful approach in identifying the structural determinants of functional differences between leaf and root Fd proteins.

SUPPORTING INFORMATION AVAILABLE

Figure depicting structural changes from initial models upon relaxation. This material is available free of charge via the Internet at http://pubs.acs.org.

REFERENCES

1. Cammack, R., Rao, K. K., Bargeron, C. P., Hutson, K. G., Andrew, P. W., and Rogers, L. J. (1977) Midpoint redox potentials of plant and algal ferredoxins, *Biochem. J. 168*, 205−9.
2. Arnon, D. I. (1988) The discovery of ferredoxin: the photosynthetic path, *Trends Biochem. Sci. 13*, 30−3.
3. Knaff, D. (1996) Ferredoxin and ferredoxin dependent enzymes, in *Oxygenic photosynthesis: The light reactions* (Ort, D., and Yocum, C., Eds.) pp 333−361, Kluwer Academic Publishers, Dordrecht.
4. Suzuki, A., Oaks, A., Jacquot, J. P., Vidal, J., and Gadal, P. (1985) An Electron Transport System in Maize Roots for Reactions of Glutamate Synthase and Nitrite Reductase: Physiological and Immunochemical Properties of the Electron Carrier and Pyridine Nucleotide Reductase, *Plant Physiol. 78*, 374−378.
5. Hase, T., Kimata, Y., Yonekura, K., Matsumura, T., and Sakakibara, H. (1991) Molecular Cloning and Differential Expression of the Maize Ferredoxin Gene Family, *Plant Physiol. 96*, 77−83.
6. Wada, K., Onda, M., and Matsubara, H. (1986) Ferredoxin isolated from plant non-photosynthetic tissues: purification and characterization, *Plant Cell Physiol. 27*, 407−415.
7. Onda, Y., Matsumura, T., Kimata-Ariga, Y., Sakakibara, H., Sugiyama, T., and Hase, T. (2000) Differential interaction of maize root ferredoxin:NADP(+) oxidoreductase with photosynthetic and non-photosynthetic ferredoxin isoproteins, *Plant Physiol. 123*, 1037−45.
8. Hanke, G. T., Kimata-Ariga, Y., Taniguchi, I., and Hase, T. (2004) A post genomic characterization of Arabidopsis ferredoxins, *Plant Physiol. 134*, 255−64.
9. Akashi, T., Matsumura, T., Ideguchi, T., Iwakiri, K., Kawakatsu, T., Taniguchi, I., and Hase, T. (1999) Comparison of the electrostatic binding sites on the surface of ferredoxin for two ferredoxin-dependent enzymes, ferredoxin-NADP(+) reductase and sulfite reductase, *J. Biol. Chem. 274*, 29399−405.
10. Okutani, S., Hanke, G. T., Satomi, Y., Takao, T., Kurisu, G., Suzuki, A., and Hase, T. (2005) Three maize leaf ferredoxin: NADPH oxidoreductases vary in subchloroplast location, expression, and interaction with ferredoxin, *Plant Physiol. 139*, 1451−9.
11. Yonekura-Sakakibara, K., Onda, Y., Ashikari, T., Tanaka, Y., Kusumi, T., and Hase, T. (2000) Analysis of reductant supply systems for ferredoxin-dependent sulfite reductase in photosynthetic and nonphotosynthetic organs of maize, *Plant Physiol. 122*, 887−94.
12. Taniguchi, I., Miyahara, A., Iwakiri, K., Hirakawa, Y., Hayashi, Y., Nishiyama, K., Akashi, T., and Hase, T. (1997) Electrochemical study of biological functions of particular evolutionary conserved amino acid residues using mutated molecules of maize ferredoxin, *Chem. Lett. 1977*, 929−30.
13. Hurley, J. K., Weber-Main, A. M., Hodges, A. E., Stankovich, M. T., Benning, M. M., Holden, H. M., Cheng, H., Xia, B., Markley, J. L., Genzor, C., Gomez-Moreno, C., Hafezi, R., and Tollin, G. (1997) Iron-sulfur cluster cysteine-to-serine mutants of Anabaena [2Fe-2S] ferredoxin exhibit unexpected redox properties and are competent in electron transfer to ferredoxin:$NADP^+$ reductase, *Biochemistry 36*, 15109−17.
14. Weber-Main, A. M., Hurley, J. K., Cheng, H., Xia, B., Chae, Y. K., Markley, J. L., Martinez-Julvez, M., Gomez-Moreno, C., Stankovich, M. T., and Tollin, G. (1998) An electrochemical, kinetic, and spectroscopic characterization of [2Fe-2S] vegetative and heterocyst ferredoxins from Anabaena 7120 with mutations in the cluster binding loop, *Arch. Biochem. Biophys. 355*, 181−8.
15. Hurley, J. K., Weber-Main, A. M., Stankovich, M. T., Benning, M. M., Thoden, J. B., Vanhooke, J. L., Holden, H. M., Chae, Y. K., Xia, B., Cheng, H., Markley, J. L., Martinez-Julvez, M., Gomez-Moreno, C., Schmeits, J. L., and Tollin, G. (1997)

Structure-function relationships in Anabaena ferredoxin: correlations between X-ray crystal structures, reduction potentials, and rate constants of electron transfer to ferredoxin:NADP+ reductase for site-specific ferredoxin mutants, *Biochemistry 36*, 11100−17.
16. Pizzitutti, F., Setif, P., and Marchi, M. (2003) Theoretical investigation of the "CO in"-"CO out" isomerization in a [2Fe-2S] ferredoxin: free energy profiles and redox states, *J. Am. Chem. Soc. 125*, 15224−32.
17. Kurisu, G., Kusunoki, M., Katoh, E., Yamazaki, T., Teshima, K., Onda, Y., Kimata-Ariga, Y., and Hase, T. (2001) Structure of the electron transfer complex between ferredoxin and ferredoxin-NADP(+) reductase, *Nat. Struct. Biol. 8*, 117−21.
18. Hanke, G. T., Kurisu, G., Kusunoki, M., and Hase, T. (2004) Fd: FNR electron transfer complexes: evolutionary refinement of structural interactions, *Photosynth. Res. 81*, 317−327.
19. Hurley, J. K., Hazzard, J. T., Martinez-Julvez, M., Medina, M., Gomez-Moreno, C., and Tollin, G. (1999) Electrostatic forces involved in orienting Anabaena ferredoxin during binding to Anabaena ferredoxin:NADP+ reductase: site-specific mutagenesis, transient kinetic measurements, and electrostatic surface potentials, *Protein Sci. 8*, 1614−22.
20. Binda, C., Coda, A., Aliverti, A., Zanetti, G., and Mattevi, A. (1998) Structure of the mutant E92K of [2Fe-2S] ferredoxin I from Spinacia oleracea at 1.7 A resolution, *Acta Crystallogr., Sect. D: Biol. Crystallogr. 54*, 1353−8.
21. Shen, B., Jollie, D. R., Stout, C. D., Diller, T. C., Armstrong, F. A., Gorst, C. M., La Mar, G. N., Stephens, P. J., and Burgess, B. K. (1994) Azotobacter vinelandii ferredoxin I. Alteration of individual surface charges and the [4FE-4S]2+/+ cluster reduction potential, *J. Biol. Chem. 269*, 8564−75.
22. Kimata, Y., and Hase, T. (1989) Localization of Ferredoxin Isoproteins in Mesophyll and Bundle Sheath Cells in Maize Leaf, *Plant Physiol. 89*, 1193−1197.
23. Standley, D. M., Toh, H., and Nakamura, H. (2005) GASH: an improved algorithm for maximizing the number of equivalent residues between two protein structures, *BMC Bioinformatics 6*, 221.
24. Morikami, K., T., N., A., K., M., S., and Nakamura, H. (1992) Presto(protein engineering simulator): A vectorized molecular mechanics program for biopolymers, *Comput. Chem. 16*, 243−8.
25. Standley, D. M., Toh, H., and Nakamura, H. (2004) Detecting local structural similarity in proteins by maximizing number of equivalent residues, *Proteins 57*, 381−91.
26. Lelong, C., Setif, P., Lagoutte, B., and Bottin, H. (1994) Identification of the amino acids involved in the functional interaction between photosystem I and ferredoxin from Synechocystis sp. PCC 6803 by chemical cross-linking, *J. Biol. Chem. 269*, 10034−9.

BI061779D